Time-resolved photoelectron imaging of $S_2 \rightarrow S_1$ internal conversion in benzene and toluene

Yoshi-Ichi Suzuki,[1,2,3] Takuya Horio,[1,2,3] Takao Fuji,[1,3,a)] and Toshinori Suzuki[1,2,3,b)]
[1]*Japan Science and Technology Agency, CREST, Sanbancho, Chiyoda-ku, Tokyo 102-0075, Japan*
[2]*Department of Chemistry, Graduate School of Science, Kyoto University, Kyoto 606-8502, Japan*
[3]*Chemical Dynamics Laboratory, RIKEN Advanced Science Institute, 2-1 Hirosawa, Wako 351-0198, Japan*

(Received 18 February 2011; accepted 13 April 2011; published online 12 May 2011)

Ultrafast internal conversion of benzene and toluene from the S_2 states was studied by time-resolved photoelectron imaging with a time resolution of 22 fs. Time−energy maps of the photoelectron intensity and the angular anisotropy were generated from a series of photoelectron images. The photoelectron kinetic energy distribution exhibits a rapid energy shift and intensity revival, which indicates nuclear motion on the S_2 adiabatic surface, while the ultrafast evolution of the angular anisotropy revealed a change in the electronic character of the S_2 adiabatic surface. From their decay profiles of the total photoelectron intensity, the time constants of 48 ± 4 and 62 ± 4 fs were determined for the population decay from the S_2 states in benzene and toluene, respectively. © *2011 American Institute of Physics*. [doi:10.1063/1.3586809]

I. INTRODUCTION

Conical intersection (CI) of potential energy surfaces (PESs) facilitates ultrafast internal conversion in polyatomic molecules.[1] When CI occurs near the bottom of the upper diabatic PES, ultrafast internal conversion occurs from the upper to lower diabatic state within a vibrational period.[1] This ultrafast quenching process converts electronic energy into heat (vibrational energy) and this plays an essential role in ensuring the photostability of DNA bases.[2]

With the exception of highly excited vibronic states in the channel three region,[3–8] the $S_1(^1B_{2u})$ electronic state of benzene is long lived with a lifetime of ca. 90 ns.[9,10] On the other hand, the second singlet excited state $S_2(^1B_{1u})$ of benzene is extremely short lived, as evidenced by a broad, structureless $S_2 \leftarrow S_0$ UV absorption spectrum even at ultralow temperatures.[11] To understand the dynamics of these excited states, it is essential to investigate CIs.[12–15] The minimum-energy structure of benzene in the S_2 state has been predicted to be a boat form;[12,13] consequently, a photoexcited S_2 molecule will deform very rapidly from a planar structure in the Franck−Condon state to non-planar structures. By performing multiconfiguration self-consistent-field calculations, Palmer *et al.* predicted that the S_2-S_1 minimum-energy conical intersection (MECI) point is located at the out-of-plane bent structure (prefulvenic form) near the minimum-energy structure of S_2.[13] The adiabatic PES of the S_2 $(^1B_{2u})$ state is formed by avoided crossings of several electronic states; it has the ionic character in the Franck−Condon region,[16] while it changes to covalent near the S_2-S_1 CI.[13] Thus, the photoexcited wave packet on the S_2 PES will acquire the $^1E_{2g}$ electronic character[12,13] during nuclear motion toward CI. By performing CASPT2 calculations, Toniolo *et al.* confirmed that the Franck−Condon region is energetically higher than the S_2-S_1 MECI point, as predicted previously, and they showed that the S_2 state decays to the S_1 state through CI in less than 100 fs.[14] After S_2-S_1 internal conversion, the molecule undergoes further internal conversion to S_0 and photochemical isomerization to various molecular forms, including Dewar benzene.[17,18]

In the 1990s, Radloff *et al.*[19–21] investigated the internal conversion from the S_2 state of benzene using time-resolved photoelectron spectroscopy (TRPES).[22–27] They observed that the photoexcited S_2 state changes to S_1 within 40 ± 10 fs and that vibrationally excited S_1 states created by internal conversion further decay within 6.7 ± 0.3 ps.[21,28] Similar experiments on toluene yielded lifetimes of 50 ± 10 fs in S_2 and 4.3 ± 0.2 ps in S_1.[28] Lee *et al*. obtained lifetimes of 43–54 fs and 9.4–88 ps, respectively, for S_2 and S_1 of benzene derivatives such as indene, styrene, and phenylacetylene using TRPES.[29] Liu *et al.* have recently measured the lifetime of the S_2 state of o-xylene to be ca. 60 fs by two-photon excitation with a 400-nm pulse to S_2 and single-photon ionization with a 266-nm pulse.[30] They estimated the average lifetime of vibrationally excited S_1 molecules created by CI to be 9.9 ps.[30] These results suggest that benzene derivatives have common dynamics of internal conversion from S_2 state within 100 fs and subsequent picosecond decay of the vibrationally excited S_1 state. Although the estimates of the time constants reported so far seem to be reasonably accurate, the limited time resolution (>100 fs)[20,21,28–30] did not allow observation of the real-time wave packet motions on the PESs.

The objective of the present study is to gain further insights into ultrafast internal conversion of benzene and substituted benzene (toluene) from the S_2 state by producing time−energy maps of the photoelectron intensity and photoelectron angular anisotropy[31–33] with a time resolution of 22 fs.[34] The photoelectron angular distribution (PAD)

a)Present address: Institute for Molecular Science, Myodaiji, Okazaki 444-8585, Japan.
b)Author to whom correspondence should be addressed. Electronic mail: suzuki@kuchem.kyoto-u.ac.jp.

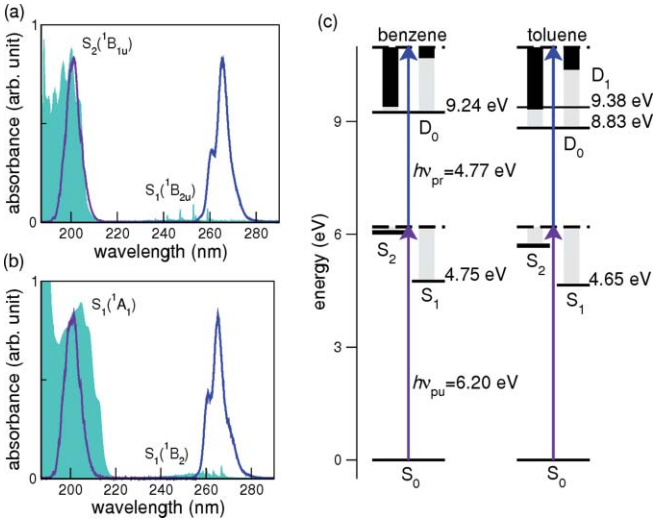

FIG. 1. UV photoabsorption spectra of (a) benzene and (b) toluene at room temperature (shaded region). The solid lines indicate the spectra of the pump and probe pulses. (c) Schematic energy diagrams of benzene and toluene. The gray and black bars indicate the maximum vibrational energy and the corresponding photoelectron kinetic energy, respectively. The origin bands of the S_2 states of benzene and toluene were estimated to be ca. 6.03 and 5.7 eV, respectively. The vertical excitation energy of the D_1 state of toluene is 9.38 eV, while the adiabatic energy is not known.

only obtainable with time-resolved photoelectron imaging (TRPEI)[33–37] provides valuable information on the electronic dynamics in photoexcited molecules.[38]

II. EXPERIMENT

The TRPEI setup has been described in detail elsewhere.[39] The pump (200 nm) and probe (260 nm) pulses were generated from a multicolor filamentation light source[40,41] based on a cryogenically cooled Ti:sapphire amplifier (pulse energy: 2 mJ; pulse length: 25 fs; wavelength: 780 nm; repetition rate: 1 kHz). The two pulses from the filamentation cell were compressed by grating compressors.[40] The pulse widths were measured to be 14 fs (260 nm) and 17 fs (200 nm).[42] The two pulses were vertically displaced after the grating compressor and the delay time (t) between them was controlled with a closed-loop translation stage. The pump and probe pulses were focused by a concave mirror (r = 1500 mm) onto a supersonic molecular beam of benzene (~9%) or toluene (~3%) seeded in He carrier gas (stagnation pressure: 760 Torr). The intersection angle between the pump and probe pulses was ~0.8°. To prevent one-color multiphoton processes, the pump and probe pulse energies were, respectively, reduced to 20 nJ/pulse (200 nm) and 250 nJ/pulse (260 nm) by variable apertures.

Figure 1 shows the spectra of the 200-nm pump and 260-nm probe pulses overlaid with the UV absorption spectra of benzene and toluene at room temperature. (The symmetry notations indicated for toluene are of the C_{2v} point group[43] that neglects the three-fold symmetry of the methyl group.) For both molecules, the pump pulse spectrum overlaps well with the $S_2 \leftarrow S_0$ absorption spectrum. Note that a part of the probe pulse overlaps with a weak $S_1 \leftarrow S_0$ absorption spectrum, which in principle could lead to time-dependent ionization signals due to a probe−pump process in the negative time range. However, the $S_1 \leftarrow S_0$ absorption cross section is very small so that the signal in the negative time range was negligible in our experiments.

Photoelectrons generated by $(1+1')$ resonance-enhanced multiphoton ionization were accelerated in the molecular beam propagation direction and projected onto a two-dimensional position-sensitive detector consisting of a dual microchannel plate (75 mmϕ), a phosphor screen (P46), and an image-intensified charge-coupled device camera (Andor, *i*-Star; 1024 × 1024 pixels). The polarization directions of the pump and probe beams were aligned parallel to each other and they were parallel to the face of the microchannel plate detector. Images were measured at 5 fs intervals in a delay time and the acquisition time at each delay in a single scan was 13 s. Sixty-five images were measured successively in a single scan from −50 to 275 fs and 10 scans were performed.[44] The three-dimensional photoelectron velocity and angular distributions were reconstructed from the observed projection images using the pBaseX method.[45]

The photoelectron kinetic energy (PKE) was calibrated by observing one-color three-photon ionization of Xe at 260 nm. The ultimate energy resolution of our photoelectron imaging system is limited to 0.25 eV (full width at half maximum) by the broad spectra of the pump and probe pulses. The cross-correlation of the pump and probe pulses was confirmed *in situ* to be 22 fs by nonresonant $(1+1')$ multiphoton ionization of ethanol seeded in a supersonic jet of Ar. The time origin ($t = 0$) of the pump−probe delay was determined with an accuracy of a few femtoseconds (~2 fs) from the cross-correlation trace.

III. RESULTS

In $(1 + 1')$ resonance enhanced multiphoton ionization with the polarization vectors of the pump and probe beams parallel to each other, the time-dependent photoionization differential cross section $I(t, E, \theta)$ can be expressed as

$$I(t, E, \theta) = \frac{\sigma(t, E)}{4\pi}\{1 + \beta_2(t, E)P_2(\cos\theta) + \beta_4(t, E)P_4(\cos\theta)\}, \quad (1)$$

where E is the PKE, θ is the angle between the electron momentum and the laser polarization direction, and $P_n(x)$ is the nth-order Legendre polynomial. Integrating Eq. (1) over the PKE and the angle yields the time-dependent photoionization signal, $I(t)$, which can be measured as the total signal intensity of photoelectrons at a certain delay time. Integrating Eq. (1) over only the angle yields the time-dependent photoelectron kinetic energy distribution (PKED), $\sigma(t,E)$.

A. Total photoelectron signal intensity

Figures 2(a) and 2(b) show the time profiles of the photoionization signal intensity observed for benzene and toluene, respectively. The measured time profiles for the electron (circles) and ion (triangles) signals are in excellent

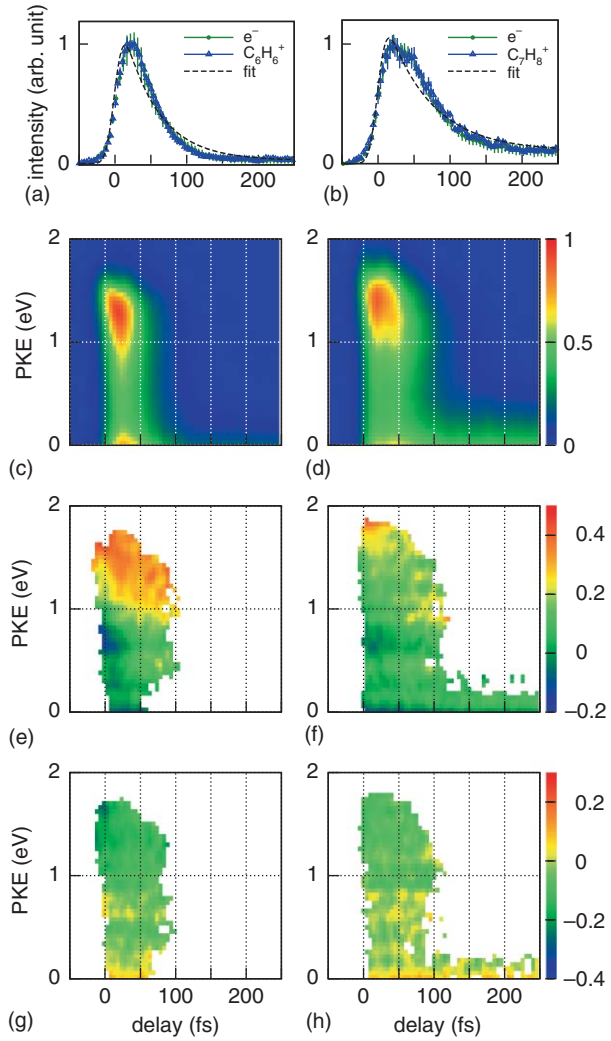

FIG. 2. The time profiles of the photoionization signal intensity for (a) benzene and (b) toluene. Photoelectron and ion ($C_6H_6^+$ or $C_7H_8^+$) signals are indicated by green circles and blue triangles, respectively. Time-energy maps of the photoelectron intensity, $\sigma(t, E)$, for (c) benzene and (d) toluene. Time-energy maps of the photoelectron angular anisotropies, $\beta_2(t, E)$, for (e) benzene and (f) toluene and $\beta_4(t, E)$ for (g) benzene and (h) toluene. Data points for β_2 and β_4 with standard deviations smaller than 0.2 are shown (see text).

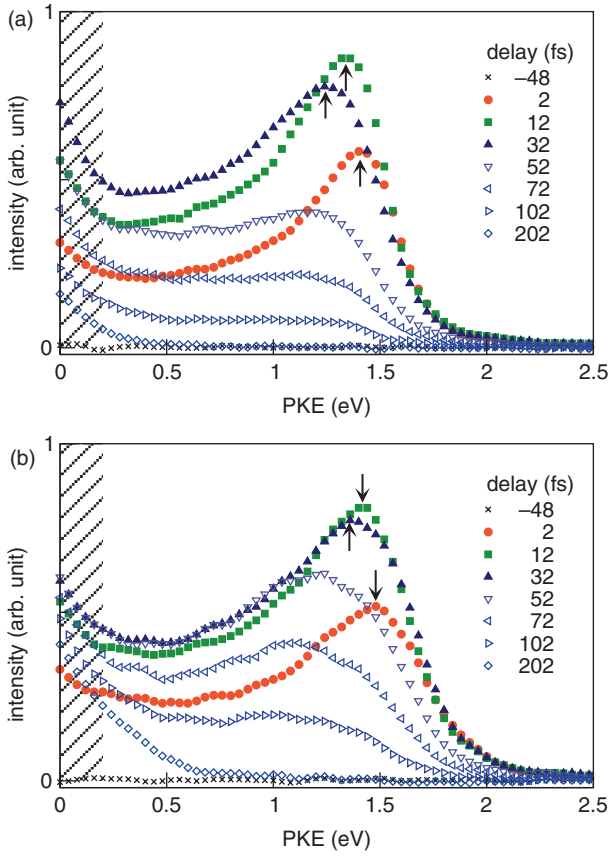

FIG. 3. PKEDs at different delay times for (a) benzene and (b) toluene. Arrows denote the peak positions at $t = 2$, 12, and 32 fs. The intensities below 0.2 eV (shaded region) may have relatively large errors.

agreement, which is consistent with cluster and fragment ions not being detected in the time-of-flight mass spectra.

The time profiles in Figs. 2(a) and 2(b) exhibit a rapid decay within 100 fs and a small plateau that remains for a considerably longer time. As described in the introduction, previous theoretical studies have suggested that cascading internal conversion occurs from $S_2 \rightarrow S_1 \rightarrow S_0$ via CIs.[13,14] We performed curve fitting of the observed time profiles using a single exponential decay function, $\exp(-t/\tau)$, with a time constant τ and a corresponding exponential rise expressed by $1-\exp(-t/\tau)$. The lifetime of vibrationally excited S_1 is sufficiently long (>4 ps) to exclude it from the fitting parameters. The apparatus function (Gaussian with a full width at half maximum of 22 fs) was accounted for in the fitting. The fitted curves are indicated by the broken lines in Figs. 2(a) and 2(b). The time constants τ of benzene and toluene were, respectively, estimated to be 48 ± 4 and 62 ± 4 fs, which are in agreement with 40 ± 10 and 50 ± 10 fs estimated by Radloff *et al.*[21,28] Comparing the results for benzene and toluene, the lifetime of S_2 was slightly increased by methylation, which is qualitatively consistent with a slower nuclear motion with increased effective inertia in toluene. On the other hand, close examination of the fitted curves [Figs. 2(a) and 2(b)] reveals that a single exponential model does not adequately reproduce the observed time profiles. We will return to this point in a later section.

B. PKED

Figures 2(c) and 2(d) show time-energy maps of PKED produced for benzene and toluene, respectively. These figures indicate that the fast-decaying and long-lived components in Figs. 2(a) and 2(b) have considerably different kinetic energy distributions. Close examination of the high-energy (PKE: 1–1.5 eV) regions in Figs. 2(c) and 2(d) reveals that the peak positions of the high-energy components continuously shift to a lower energy from the moment the signals initially appear: this shift is clearer in Fig. 3, which displays the PKEDs on expanded scales. The shift is a manifestation of the vibrational wave packet motion on the S_2 surface. Since the equilibrium structures of benzene and toluene are very similar between S_0 and D_0,[46] photoionization from the Franck–Condon state in S_2 should occur to low vibrational levels in D_0, resulting in a high PKE. On the other hand, since the minimum-energy structure in S_2 is the boat form, the Franck–Condon state on

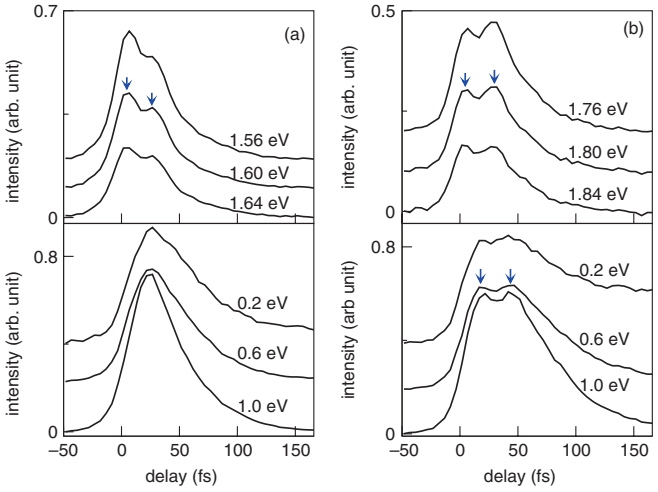

FIG. 4. Time evolutions of photoelectron intensities at different kinetic energies for (a) benzene and (b) toluene. Arrows indicate the time intervals between the double peaks observed in the time profiles at 1.6 eV for benzene and at 0.6 and 1.8 eV for toluene.

S_2 is unstable with respect to out-of-plane deformation[13–15] and the wave packet immediately moves in this direction. This motion rapidly increases the vibrational energy and consequently induces photoionization to higher vibrational levels in D_0.

Figure 4 shows time profiles for the photoelectron intensities, $\sigma(t, E)$, in different PKE subsections. Close examination of this figure reveals that the photoelectron intensities of both benzene and toluene revive at $t > 20$ fs. These revival structures are ascribed to wave packet motion in the direction perpendicular to the out-of-plane distortion that has the steepest decent on the S_2 PES. For benzene [Fig. 4(a)], the revival peak is most clearly visible at a PKE of 1.6 eV. The time interval between the two peaks is ca. 20 fs, which corresponds to approximately 1700 cm^{-1} in the energy domain. Similar peaks are seen for toluene [Fig. 4(b)] with a separation of ca. 24 fs (1400 cm^{-1}) at a short time delay and a PKE of 1.8 eV. For toluene at 0.6 eV, two peaks with the same separation (24 fs) have a lag time of 10 fs relative to the peaks at 1.8 eV.

C. Photoelectron angular distributions

The time-dependent photoelectron angular anisotropy parameters, $\beta_2(t, E)$ and $\beta_4(t, E)$, are displayed as 2D time−energy maps in Fig. 2 for benzene and toluene. Since β_2 and β_4 cannot be accurately determined when the signal is too low, the figure shows only values that have standard deviations of less than 0.2 (estimated from 10 measurements).

Close examination of Fig. 2(e) for benzene reveals that β_2 exhibits a clear time dependence, especially around 0.7 eV where β_2 is negative at $t = 0$ and gradually increases with time, becoming positive around ca. 30 fs. In addition, the time dependence of β_2 is apparent in Fig. 2(f) for toluene, especially around 1.0 eV. To examine the early time behavior, Fig. 5 shows $\beta_2(t, E)$ for benzene and toluene from −10 to 100 fs at 0.7 and 1.0 eV. This figure shows that β_2 starts to increase from $t = 0$ fs.

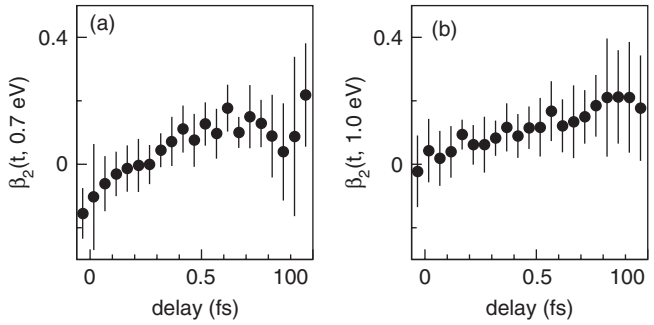

FIG. 5. Time evolutions of the photoelectron anisotropy parameter $\beta_2(t)$ (circles) of (a) benzene and (b) toluene. The error bars correspond to the standard deviations (1σ) estimated from 10 measurements.

IV. DISCUSSION

A. Ultrafast dynamics in S_2 state

The rapid increases in $\beta_2(t, E)$ clearly indicates that the electronic character changes along the reaction path. The S_2 diabatic surface has a gradient along out-of-plane distortions such as Q_4 (b_{2g}, boat) and Q_{16} (e_{2u}, chair), whereas S_3 ($^1E_{1u}$) and S_4 ($^1E_{2g}$) are stabilized more rapidly by out-of-plane distortions than S_2. Consequently, it is likely that the S_2 PES undergoes an avoided crossing with these upper state surfaces, and the resulting S_2 adiabatic surface changes its electronic character along these coordinates (Fig. 6). Meisl and Janoschek[12] and Palmer *et al.*[13] studied the minimum energy region of the adiabatic S_2 PES and suggested that the electronic character changes from $S_2(^1B_{1u})$ to $S_4(^1E_{2g})$ along a reaction path for internal conversion (Fig. 6). On the other hand, PES from the Franck-Condon region to the minimum energy region has not been fully investigated. In the Franck-Condon region, the electron configuration of $S_4(^1E_{2g})$ is dominated by the $a_{2u}(\pi) \rightarrow e_{2u}(\pi^*)$ and $e_{1g}^2(\pi^2) \rightarrow e_{2u}^2(\pi^{*2})$ configurations.[16] Ionization to $D_0(e_{1g}^{-1})$ is forbidden from these two configurations, assuming Koopmans' correlation,

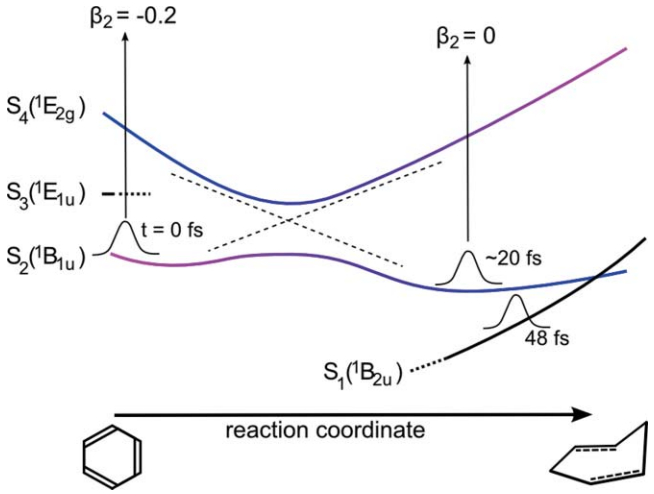

FIG. 6. Schematic potential energy curves of benzene along the reaction coordinate from the D_{6h} equilibrium geometry (Kekule benzene) to the S_2-S_1 MECI (prefulvenic form). The figure was drawn by considering the avoided crossing (dashed lines) between S_2 ($^1B_{1u}$) and S_4 ($^1E_{2g}$) reported by Meisl and Janoschek.[12]

so that $S_4(^1E_{2g})$ may have a rather small photoionization integral cross section. Since the observed photoelectron intensity does not decrease in the first 20 fs, the $^1E_{2g}$ state seems to come into play later near the MECI (prefulvenic form). On the other hand, the main electronic configuration of $S_3(^1E_{1u})$, $e_{1g} \rightarrow e_{2u}$,[16] is the same as S_2, and $^1E_{1u}$ is expected to have a similar integral cross section to $^1B_{1u}$. Therefore, the initial change of the photoelectron anisotropy parameter may be ascribed to involvement of the $S_3(^1E_{1u})$ character in the dynamics. Recent calculations by Penfold and Worth [15] showed that the one-dimensional PESs of $^1B_{1u}$ and $^1E_{1u}$ have the minima that are similar in energy and geometry along the Q_1 coordinate (ring breathing) and that there is a large nonadiabatic coupling between these states (0.24 eV along Q_8) at the equilibrium geometry of S_0.

The revival peak in $\sigma(t,E)$ is ascribed to wave packet motion[47–50] perpendicular to the reaction path. Previously, theoretical and experimental studies have indicated the presence of $X_0^1 1_0^n$ progressions in the 200-nm band system of benzene [Fig. 2(a)], in which ν_1 is the totally symmetric ring-breathing mode.[11,51,52] In D_{6h} symmetry, the transition $S_2(^1B_{1u})$-$S_0(^1A_{1g})$ is allowed by the vibronic coupling between $S_2(^1B_{1u})$ and $S_3(^1E_{1u})$ through e_{2g} mode.[15,53,54] Penfold and Worth calculated S_2–S_0 absorption spectrum using their theoretical PESs of S_n $(n = 0-5)$[15,55] and predicted that the $9_0^1 1_0^n$ progression is the main vibrational structure in the spectrum: ν_9 is the e_{2g} symmetric C–H bending mode. On the other hand, Hiraya and Shobatake experimentally identified four vibrational progressions for jet-cooled benzene and assigned them to 1_0^n, $6_0^1 1_0^n$, $8_0^1 1_0^n$, and $16_1^1 8_0^1 1_0^n$.[11] They assumed that the bands 1_0^n are allowed without excitation of the e_{2g} mode due to symmetry lowering to D_{2h}.[11] In any case, the benzene ring is expanded by electronic excitation but not dissociated during the dynamics. Therefore, it seems reasonable to assign the observed beat to the motion along the coordinate of ν_1. The fundamental frequency of the ν_1 mode is ca.900 cm^{-1} and our pump laser spectrum [$\sim$1740 cm^{-1} (FWHM) in Fig. 2] is sufficiently broad to coherently excite three members of each $X_0^1 1_0^n$ progression. The observed revival time corresponds to the vibrational energy difference of 1700 cm^{-1}, which reasonably agree with two-quanta of ν_1. The revival feature corresponding to one quantum of ν_1 is not clearly seen in Fig. 4(a) due to the short lifetime of S_2. The S_2 and D_0 must be different in geometry for the appearance of the revival peak; otherwise the coherently populated vibrational states in S_2 are ionized into different vibrational states of D_0, which would not cause the revival peak. According to UV (He I) photoelectron spectrum[56] and the UV absorption spectrum of benzene, D_0 is similar to S_0 in equilibrium structure while largely different from S_2. Therefore, the appearance of the revival peak in our TRPEI is consistent with the difference of the structures in S_2 and D_0.

It may be surprising that we observed a clear revival peak for toluene since it has a less structured absorption spectrum[57] [Fig. 1(b)] than benzene. The lifetime of the S_2 state of toluene we determined is longer than that of benzene, indicating that lifetime broadening of the spectrum is less significant for toluene than benzene. Thus, the broad spectrum of toluene is ascribed to congested spectral feature and hot bands due to the presence of low-frequency torsional mode of the methyl group. The vibrational temperatures in the previous photoabsorption experiments[57] were rather high ($\sim$ room temperature). Therefore, the revival peaks observed in the time domain reflect the hidden vibrational structures in the apparently broad spectrum in the frequency domain.

The revival peaks observed in the high PKE region (1.74–1.86 eV) have a similar time interval with that observed for benzene; therefore, the vibrational mode responsible for the revival is most likely the ring breathing mode ν_1. The slightly longer time interval (24 fs) than that in benzene (20 fs) is possibly due to the increased inertia of the ring breathing mode by methylation. Although the $S_2 \leftarrow S_0$ absorption spectrum of toluene has not been analyzed, the fundamental frequencies of the ν_1 mode in S_0 are 993 and 785 cm^{-1}, for benzene and toluene,[43] respectively. The ratio (993/785 = 1.26) agrees reasonably well with the observed ratio of the revival time interval (24 fs / 20 fs = 1.2). For toluene, revival peaks appeared in low PKE region ($E < 1$ eV) with the time lag of about 10 fs with respect to the peaks at 1.8 eV. The lag time originates from the traveling time of the vibrational wave packet along the reaction path and/or the ν_1 mode, as previously observed for Na_2.[47] One important difference between benzene and toluene is that D_0 of benzene is doubly degenerate and split by Jahn-Teller interactions, while the degeneracy is lifted in toluene. The D_0 and D_1 are separated by 0.5 eV in toluene. Since there is no revival structure for benzene at low PKE ($E < 1$ eV), the revival peaks observed for toluene in the low energy region may be ascribed to ionization process to D_1.

B. Photoelectron kinetic energy distribution in ionization from S_1

Toluene has a higher plateau in the photoionization intensity after 200 fs than benzene. This is due to the lower ionization energy of toluene; benzene[58] and toluene[59,60] have adiabatic ionization energies of 9.24 and 8.83 eV, respectively. Assuming that the vibrational energy is conserved on ionization [Fig. 1(c)], the PKE is estimated to be

$$\begin{aligned} \mathrm{PKE} &= h\nu_{\mathrm{pump}} + h\nu_{\mathrm{probe}} - \mathrm{IE} - \left(h\nu_{\mathrm{pump}} - E_0^{S_1}\right) \\ &= h\nu_{\mathrm{probe}} - \mathrm{IE} + E_0^{S_1}, \end{aligned} \tag{2}$$

where ν_{pump} and ν_{probe} are the frequencies of the laser pulses, IE is the molecular ionization energy, E_0 is the energy of the zero vibrational level of each electronic state, and E_{vib} is the vibrational energy of each electronic state. $E_0^{S_1}$ is 4.75 and 4.65 eV for benzene[11] and toluene,[60] respectively. Consequently, there is a 0.31 eV difference in PKE, as discussed by Radloff *et al.*[21,28]

In Fig. 2, the widths of PKEDs exceed 1 eV at short time delays, and the distributions are cut at a PKE of 0 eV. This is analogous to the situation for pyrazine studied previously[39] and it occurs since the probe photon energy is too low to cover the entire Franck−Condon envelope for photoionization.[61] Therefore, the quantum yield of S_2-S_1 internal conversion cannot be evaluated from the result. Previously, Radloff *et al.* have analyzed the time profiles by assuming identical ionization probabilities for S_2 and S_1 and estimated the

TABLE I. Correlation of angular momentum (l) and irreducible representation (Γ) of the D_{6h} and C_{2v} point group.

l	$\Gamma(D_{6h})$	$\Gamma(C_{2v})$
s	a_{1g}	a_1
p	a_{2u}, e_{1u}	a_1, b_1, b_2
d	a_{1g}, e_{1g}, e_{2g}	$2\times a_1, b_1, a_2, b_2$
f	$a_{2u}, e_{1u}, b_{1u}, b_{2u}$	$2\times a_1, 2\times b_1, a_2, 2\times b_2$
g	$a_{1g}, e_{1g}, 2\times e_{2g}, b_{1g}, b_{2g}$	$3\times a_1, 2\times b_1, 2\times a_2, 2\times b_2$

branching ratio for internal conversion from S_2 to S_1 to be 1% for benzene.[20] However, this seems a considerable underestimation as S_2 and S_1 have very different effective ionization efficiencies due to the problem described above. Parameterized, semi-empirical wave packet calculations by Toniolo *et al.* predict that sequential internal conversion of $S_2 \rightarrow S_1 \rightarrow S_0$ will occur.[14] Although other processes such as $S_2 \rightarrow S_0$ and $S_2 \rightarrow T_1$ cannot be ruled out, we consider the yield of $S_2 \rightarrow S_1$ to be much greater than 10%. The wave packet calculations by Toniolo *et al.*[14] predict the lifetime of S_2 to be less than 100 fs, which is in reasonable agreement with the experimental observations by our group and Radloff *et al.* This also supports a $S_2 \rightarrow S_1$ internal conversion yield that is much higher than 1%.

C. Photoelectron angular distribution in ionization from S_2

The observed PADs of benzene at $t = 0$ reflect the $^1B_{1u}$ character of the S_2 state. At a low (<1 eV) PKE, $\beta_2(t, E)$ is negative while $\beta_4(t, E)$ is almost zero at $t = 0$ [Figs. 2(e), 2(g), and 5(a)]. Partial wave analysis is useful at such a low energy because the centrifugal barrier, $l(l+1)/r^2$, prevents low-energy, high-angular-momentum wavefunctions penetrating into the molecular region.[62]

In D_0 ($^2E_{1g}$) $\leftarrow$ S_2 ($^1B_{1u}$) photoionization of benzene induced by an electric dipole transition in D_{6h} symmetry, the *gerade* continua of kb_{1g}, kb_{2g}, ke_{1g}, and ke_{2g} are reached from $\pi^*(e_{2u})$ orbitals. Furthermore, since the maximum angular momentum is expected to be $l = 3$ (f wave),[63] only the two channels, ke_{1g} and ke_{2g} (d waves), are possible (Table I). Thus, only two parameters [the relative amplitude (r) and the phase (φ)] are relevant for PAD, and the following expressions are obtained for the photoelectron anisotropy parameters:

$$\beta_2 = -\frac{10}{49}\cdot\frac{2+r^2+6\sqrt{2}r\cos(\varphi)}{2+r^2}, \tag{3}$$

$$\beta_4 = \frac{1}{6}\beta_2 - \frac{1}{21}. \tag{4}$$

The alignment[62,64] of S_2 molecules prepared by the S_2–S_0 transition has been taken into account (Appendix A). The S_2 ($^1B_{1u}$) $\leftarrow$ S_0 ($^1A_{1g}$) transition is allowed by Herzberg–Teller coupling between $^1B_{1u}$ and S_3 ($^1E_{1u}$) through the e_{2g} mode in the D_{6h} point group; therefore, the vibronically induced transition dipole moment of S_2 ($^1B_{1u}$) $\leftarrow$ S_0 is in the molecular plane. Equation (3) indicates that the possible range of β_2 is $-0.82 \le \beta_2 \le 0.41$, with which Eq. (4) suggests $\beta_4(t, E)$ is small. Therefore, this model explains the observed negative $\beta_2(t, E)$ and small $\beta_4(t, E)$ at low PKE. On the other hand, the linear dependence between β_2 and β_4 in Eq. (4) prevents determination of the amplitude (r) and phase (φ) from these two equations. At higher PKE (>1 eV), the observed $\beta_2(t, E)$ increases to 0.5 with increasing energy, which indicates that g waves ($l = 4$) play some roles. We speculate that the enhanced contribution of g waves in this energy range is owing to the influence of shape resonances at 3–5 eV in the ke_{2g}[63,65–67] and kb_{1g}[67] continua (Table I and Ref. 63).

Due to the lower symmetry of toluene, there are twelve partial waves with $l < 4$ (Table I) to consider in partial wave analysis. Thus, the detailed analysis is not possible without numerical calculations. However, since observed β_2 and β_4 have similarity with those of benzene (i.e., small β_4 and increasing β_2 as a function of PKE at $t = 0$), the ionization mechanism of toluene is presumably similar; i.e., d waves play the essential roles with some participation of g waves.

We recently performed (1+1) photoelectron imaging of benzene via S_1 $6^1 1^n$ (n = 0–3) vibronic levels using a nanosecond UV laser (PKE < 0.6 eV).[68] Assuming Koopmans' correlation, S_1 and S_2 have the same ionization scheme: kb_{1g}, kb_{2g}, ke_{1g}, and ke_{2g} $\leftarrow$ $\pi^*(e_{2u})$. The S_1 ($^1B_{2u}$) $\leftarrow$ S_0 is allowed by coupling with $^1E_{1u}$ through e_{2g} vibrations, and the transition dipole moment is in the plane. Since the P, Q, and R branches were not coherently excited, the molecular axis alignment was not clearly defined. Nevertheless, it is noteworthy that β_2 was negative (−0.2 to −0.6) in the observed PKE range, in qualitative agreement with this work.

V. CONCLUSION

We have performed TRPEI of jet-cooled benzene and toluene with a time-resolution of 22 fs. The molecules were excited to S_2 by a 200 nm pulse and ionized by a 260 nm pulse. The S_2 state lifetimes of benzene and toluene were determined to be 48 ± 4 and 62 ± 4, respectively. The long-lived component is ascribed to S_1 populated by internal conversion from S_2. Because of the limited Franck–Condon overlap between S_1 and D_0, hot S_1 molecules were not efficiently ionized at 260 nm, which diminished the ionization signal from S_1 relative to that from S_2. The branching ratio of internal conversion from S_2 to S_1/S_0 could not be determined in this study. A progressive shift in a high-energy peak in PKED indicates wave packet motion in S_2. The time-dependent β_2 in the first 100 fs was interpreted as a change in the electronic character on the adiabatic S_2 surface along the reaction path. In future studies, we intend to use shorter wavelength light to probe electronic dephasing to all the S_1, T_1, and S_0 states and the photochemical isomerization reaction.

ACKNOWLEDGMENTS

T. Horio thanks RIKEN for a Special Postdoctoral Research Fellowship.

APPENDIX: A DERIVATION OF EQS. (3) AND (4)

The ground state of Benzene cation, D_0 ($^2E_{1g}$), is electronically degenerate and subject to Jahn-Teller effect. However, the Jahn-Teller splitting is sufficiently small compared with our energy resolution given by femtosecond laser pulses; therefore, the possible (four) vibronic levels are indistinguishable. As a result, photoionization differential cross section [Eq. (1)] can be calculated by taking incoherent sum over these four vibronic states in D_0. The number of the indistinguishable final vibronic states are four because of the direct product of $e_{2g} \times {}^2E_{1g}$, in which e_{2g} represents one-quantum excitation of the coupling mode in S_2. The vibrational excitation of the e2g mode is conserved upon ionization to D_0 ($^2E_{1g}$). The consideration of degenerate electronic state is generally cumbersome. However, when we consider the incoherent sum over the four final states, one can perform the unitary transformation of these states for convenience in calculation, since the incoherent sum is unchanged by the transformation. This implies that we can consider $^2E_{1g}$ state as $^2E_{1g}(yz)$ and $^2E_{1g}(xz)$ separately. Likewise, e_{2g} can be considered as $e_{2g}(xy)$ and $e_{2g}(x^2 - y^2)$. Here, we defined the molecular frame axes as shown below.

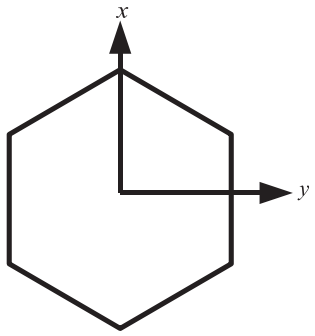

Then, we consider the following four final states of the ion core: $e_{2g}(xy) \times {}^2E_{1g}(yz)$, $e_{2g}(xy) \times {}^2E_{1g}(xz)$, $e_{2g}(x^2 - y^2) \times {}^2E_{1g}(yz)$, and $e_{2g}(x^2 - y^2) \times {}^2E_1(xz)$. And, we use these symmetry properties to sort out the possible scattering electron states and the corresponding transition dipole moments. Another consequence of the indistinguishability of the final states is that the alignment of the $S_2(^1B_{1u})$ can be considered rather easily. The $S_2 \leftarrow S_0$ transition is induced by intensity-borrowing and its transition dipole is the same as $S_3(E_{1u}) \leftarrow S_0$. The molecular alignment created by an electronic transition to the doubly degenerate state seems complex; however, examination of the theoretical expression of the photoionization differential cross section reveals that when we take the incoherent sum of the final vibronic states, the transition dipole moments to S_2 can be evaluated with the most convenient choice of the orthogonal molecular axis directions. Thus, we take $E_{1u}(x)$ and $E_{1u}(y)$ into consideration separately. In other word, we can evaluate the benzene molecules with the molecular x-axis or y-axis aligned in the laboratory frame separately. Thus, the molecular axis alignment created in the S_2 state can be assumed to be the same as x^2 or y^2. Combining the above considerations for the pumping and ionization steps, one can perform calculations of the photoionization differential cross sections for the x-polarized S_2-S_0 transition dipole coupled with ionization to two cation vibronic states $[e_{2g}(xy) \times {}^2E_{1g}]$ and the y-polarized transition dipole coupled with ionization to the other two cation vibronic states $[e_{2g}(x^2 - y^2) \times {}^2E_{1g}]$. For each case, the photoelectron anisotropy parameters expected for ionization using linearly polarized pump and probe laser beams in parallel polarization geometry are obtained by the following formula:[62]

$$\sigma_0\beta_n = \sqrt{[n]} \sum_{K,\Lambda,p,k_\gamma} (-1)^n \begin{pmatrix} K & n & k_\gamma \\ 0 & 0 & 0 \end{pmatrix} \times \rho^{\gamma_{pr}}_{k_\gamma,0} A^{\gamma_{pu}}_{K,0,\Lambda,p}(t) b_{K,n,k_\gamma,\Lambda,p}(E) \tag{A1}$$

and

$$\begin{aligned} b_{K,n,k_\gamma,\Lambda,p}(E) = \sum_{ll'} \sum_{\lambda\lambda'} \sum_{ss'} & \sqrt{3[l][l'][n][k_\gamma]} \\ & \times \frac{(-1)^{1+s+\lambda'+K}}{\sqrt{2(1+\delta_{0,\Lambda})}} \begin{pmatrix} l & l' & n \\ 0 & 0 & 0 \end{pmatrix} \\ & \times \sum_{\Lambda_L,\lambda_\gamma} \begin{pmatrix} l & l' & n \\ \lambda & -\lambda' & \Lambda_L \end{pmatrix} \begin{pmatrix} 1 & 1 & n \\ -s & s' & \lambda_\gamma \end{pmatrix} \\ & \times \left[\begin{pmatrix} n & K & k_\gamma \\ \Lambda_L & \Lambda & \lambda_\gamma \end{pmatrix} \right. \\ & \left. + (-1)^p \begin{pmatrix} n & K & k_\gamma \\ \Lambda_L & -\Lambda & \lambda_\gamma \end{pmatrix} \right] \\ & \times J_{l\lambda s}(E) J^*_{l'\lambda' s'}(E), \end{aligned} \tag{A2}$$

where $\beta_0 \equiv 1$, $[x] = 2x+1$, (:::) denotes the $3j$ symbol, $\rho^{\gamma_{pr}}_{k_\gamma,0}$ are state multipoles of probe light ($\rho^{\gamma_{pr}}_{0,0} = 1/\sqrt{3}$ and $\rho^{\gamma_{pr}}_{2,0} = -\sqrt{2/3}$ otherwise $\rho^{\gamma_{pr}}_{k_\gamma,0} = 0$), $A^{\gamma_{pu}}_{K,0,\Lambda,p}$ are alignment parameters of molecular axis, and $J_{l\lambda s}$ are the bound-free transition dipole moments. l and λ denote the quantum number of angular momentum of a photoelectron and its projection onto the molecular z axis and s denotes a component of spherical dipole operator ($s = 0, \pm 1$). The alignment parameters are deduced from the axis distributions of x^2 and y^2: $A^{\gamma_{pu}}_{0,0,0,0} = 1$, $A^{\gamma_{pu}}_{2,0,0,0} = -1$, and $A^{\gamma_{pu}}_{2,0,2,0} = \sqrt{3}$ and $-\sqrt{3}$ for x^2 and y^2, respectively, and otherwise $A^{\gamma_{pu}}_{K,0,\Lambda,p} = 0$. As noted in Sec. IV C, the nonzero $J_{l\lambda s}$ with $l < 4$ can be expressed by two parameters, r and φ, as

$$J_{2,-1,1} = -J_{2,1,-1} \equiv 1 \quad \text{and} \quad J_{2,-2,0} = -J_{2,2,0} \equiv re^{i\varphi}, \tag{A3}$$

for $^2E_{1g}(xz)$ and

$$J_{2,-1,1} = J_{2,1,-1} \equiv i \text{ and } J_{2,-2,0} = J_{2,2,0} \equiv ire^{i\varphi}, \tag{A4}$$

for $^2E_{1g}(yz)$. Using Eqs. (A2)–(A4), we obtained the same $\sigma_0\beta_n$ from Eq. (A1) for four cases. Therefore, the total sum of the photoionization differential cross sections provides also the same β_2 and β_4 that are Eqs. (3) and (4), respectively.

[1] *Conical Intersections: Electronic Structure, Dynamics & Spectroscopy* (*Advanced Series in Physical Chemistry*), edited by W. Domcke, D. R. Yarkony, and H.Köppel (World Scientific, Singapore, 2004).
[2] A. L. Sobolewski and W. Domcke, Eur. Phys. J. D **20**, 369 (2002).
[3] K. G. Spears and S. A. Rice, J. Chem. Phys. **55**, 5561 (1971).

[4]E. Riedle, H. J. Neusser, and E. W. Schlag, J. Phys. Chem. **86**, 4847 (1982).
[5]D. O'Connor, M. Sumitani, Y. Takagi, N. Nakashima, K. Kamogawa, Y. Udagawa, and K. Yoshihara, J. Phys. Chem. **87**, 4848 (1983).
[6]M. Sumitani, D. V. O'Connor, Y. Takagi, and K. Yoshihara, Chem. Phys. Lett. **108**, 11 (1984).
[7]Y. Achiba, A. Hiraya, and K. Kimura, J. Chem. Phys. **80**, 6047 (1984).
[8]J. M. Smith, X. Zhang, and J. L. Knee, J. Phys. Chem. **99**, 1768 (1995).
[9]J. Callomon, J. Parkin, and R. Lopez-Delgado, Chem. Phys. Lett. **13**, 125 (1972).
[10]T. A. Stephenson and S. A. Rice, J. Chem. Phys. **81**, 1073 (1984).
[11]A. Hiraya and K. Shobatake, J. Chem. Phys. **94**, 7700 (1991).
[12]M. Meisl and R. Janoschek, J. Chem. Soc., Chem. Commun. **1986**, 1066 (1986).
[13]I. J. Palmer, I. N. Ragazos, F. Bernardi, M. Olivucci, and M. A. Robb, J. Am. Chem. Soc. **115**, 673 (1993).
[14]A. Toniolo, A. L. Thompson, and T. J. Martínez, Chem. Phys. **304**, 133 (2004).
[15]T. J. Penfold and G. A. Worth, J. Chem. Phys. **131**, 064303 (2009).
[16]J. M. O. Matos, B. O. Roos, and P.-A. Malmqvist, J. Chem. Phys. **86**, 1458 (1987).
[17]H. R. Ward and J. S. Wishnok, J. Am. Chem. Soc. **90**, 1085 (1968).
[18]D. Bryce-Smith, A. Gilbert, and D. A. Robinson, Angew. Chem., Int. Ed. Engl. **10**, 745 (1971).
[19]W. Radloff, T. Freudenberg, H. H. Ritze, V. Stert, K. Weyers, and F. Noack, Chem. Phys. Lett. **245**, 400 (1995).
[20]W. Radloff, T. Freudenberg, H. H. Ritze, V. Stert, F. Noack, and I. V. Hertel, Chem. Phys. Lett. **261**, 301 (1996).
[21]W. Radloff, V. Stert, T. Freudenberg, I. Hertel, C. Jouvet, C. Dedonder-Lardeux, and D. Solgadi, Chem. Phys. Lett. **281**, 20 (1997).
[22]D. Neumark, Annu. Rev. Phys. Chem. **52**, 255 (2001).
[23]A. Stolow, Annu. Rev. Phys. Chem. **54**, 89 (2003).
[24]I. V. Hertel and W. Radloff, Rep. Prog. Phys. **69**, 1897 (2006).
[25]K. L. Reid, Int. Rev. Phys. Chem. **27**, 607 (2008).
[26]R. S. Minns, D. S. N. Parker, T. J. Penfold, G. A. Worth, and H. H. Fielding, Phys. Chem. Chem. Phys. **12**, 15607 (2010).
[27]A. D. G. Nunn, R. S. Minns, R. Spesyvtsev, M. J. Bearpark, M. A. Robb, and H. H. Fielding, Phys. Chem. Chem. Phys. **12**, 15751 (2010).
[28]P. Farmanara, V. Stert, W. Radloff, and I. Hertel, J. Phys. Chem. A **105**, 5613 (2001).
[29]S.-H. Lee, K.-C. Tang, I.-C. Chen, M. Schmitt, J. P. Shaffer, T. Schultz, J. G. Underwood, M. Z. Zgierski, and A. Stolow, J. Phys. Chem. A **106**, 8979 (2002).
[30]Y. Liu, B. Tang, H. Shen, S. Zhang, and B. Zhang, Opt. Express **18**, 5791 (2010).
[31]T. Seideman, Annu. Rev. Phys. Chem. **53**, 41 (2002).
[32]K. L. Reid, Annu. Rev. Phys. Chem. **54**, 397 (2003).
[33]T. Suzuki, Annu. Rev. Phys. Chem. **57**, 555 (2006).
[34]T. Horio and T. Suzuki, Rev. Sci. Instrum. **80**, 013706 (2009).
[35]J. A. Davies, R. E. Continetti, D. W. Chandler, and C. C. Hayden, Phys. Rev. Lett. **84**, 5983 (2000).
[36]M. Tsubouchi, B. J. Whitaker, L. Wang, H. Kohguchi, and T. Suzuki, Phys. Rev. Lett. **86**, 4500 (2001).
[37]A. E. Bragg, J. R. R. Verlet, A. Kammrath, O. Cheshnovsky, and D. M. Neumark, Science **306**, 669 (2004).
[38]T. Horio, T. Fuji, Y.-I. Suzuki, and T. Suzuki, J. Am. Chem. Soc. **131**, 10392 (2009).
[39]Y.-I. Suzuki, T. Fuji, T. Horio, and T. Suzuki, J. Chem. Phys. **132**, 174302 (2010).
[40]T. Fuji, T. Suzuki, E. E. Serebryannikov, and A. Zheltikov, Phys. Rev. A **80**, 063822 (2009).
[41]T. Fuji, T. Horio, and T. Suzuki, Opt. Lett. **32**, 2481 (2007).
[42]M. Li, J. P. Nibarger, C. Guo, and G. N. Gibson, Appl. Opt. **38**, 5250 (1999).
[43]C. G. Hickman, J. R. Gascooke, and W. D. Lawrance, J. Chem. Phys. **104**, 4887 (1996).
[44]See supplementary material at http://dx.doi.org/10.1063/1.3586809 for animation of photoelectron images.
[45]G. A. Garcia, L. Nahon, and I. Powis, Rev. Sci. Instrum. **75**, 4989 (2004).
[46]R. Lindner, K. Muller-Dethlefs, E. Wedum, K. Haber, and E. R. Grant, Science **271**, 1698 (1996).
[47]M. Wollenhaupt, V. Engel, and T. Baumert, Annu. Rev. Phys. Chem. **56**, 25 (2005).
[48]M. Seel and W. Domcke, J. Chem. Phys. **95**, 7806 (1991).
[49]Y. Arasaki, K. Takatsuka, K. Wang, and V. McKoy, J. Chem. Phys. **132**, 124307 (2010).
[50]Y. Arasaki and K. Takatsuka, Phys. Chem. Chem. Phys. **12**, 1239 (2010).
[51]B. Katz, M. Brith, B. Sharf, and J. Jortner, J. Chem. Phys. **52**, 88 (1970).
[52]E. Pantos, A. M. Taleb, and T. D. S. Hamilton, Mol. Phys. **28**, 1139 (1974).
[53]R. J. Sension, R. J. Brudzynski, S. Li, B. S. Hudson, F. Zerbetto, and M. Z. Zgierski, J. Chem. Phys. **96**, 2617 (1992).
[54]G. Worth, J. Photochem. Photobiol, A **190**, 190 (2007).
[55]T. J. Penfold, *Simulating and controlling non-adiabatic effects in ultrafast photochemistry*, PhD thesis, University of Birmingham, 2009.
[56]P. Baltzer, L. Karlsson, B. Wannberg, G. Öhrwall, D. M. P. Holland, M. A. MacDonald, M. A. Hayes, and W. von Niessen, Chem. Phys. **224**, 95 (1997).
[57]A. Bolovinos, J. Philis, E. Pantos, P. Tsekeris, and G. Andritsopoulos, J. Mol. Spectrosc. **94**, 55 (1982).
[58]G. Nemeth, H. Selzle, and E. Schlag, Chem. Phys. Lett. **215**, 151 (1993).
[59]W. D. Geppert, C. E. H. Dessent, M. C. R. Cockett, and K. Müller-Dethlefs, Chem. Phys. Lett. **303**, 194 (1999).
[60]K. T. Lu, G. C. Eiden, and J. C. Weisshaar, J. Phys. Chem. **96**, 9742 (1992).
[61]S. Y. Liu, Y. Ogi, T. Fuji, K. Nishizawa, T. Horio, T. Mizuno, H. Kohguchi, M. Nagasono, T. Togashi, K. Tono, M. Yabashi, Y. Senba, H. Ohashi, H. Kimura, T. Ishikawa, and T. Suzuki, Phys. Rev. A **81**, 031403 (2010).
[62]Y.-I. Suzuki and T. Suzuki, Mol. Phys. **105**, 1675 (2007).
[63]Y.-I. Suzuki and T. Suzuki, J. Phys. Chem. A **112**, 402 (2008).
[64]Y. Suzuki, M. Stener, and T. Seideman, J. Chem. Phys. **118**, 4432 (2003).
[65]I. Wilhelmy, L. Ackermann, A. Görling, and N. Rösch, J. Chem. Phys. **100**, 2808 (1994).
[66]M. Venuti, M. Stener, and P. Decleva, Chem. Phys. **234**, 95 (1998).
[67]T. Carlson, P. Gerard, M. O. Krause, F. Grimm, and B. Pullen, J. Chem. Phys. **86**, 6918 (1987).
[68]D. Niu, Y. Ogi, Y.-I. Suzuki, and T. Suzuki, J. Phys. Chem. A **115**, 2096 (2011).